Soil Use and Management

Soil Use and Management

doi: 10.1111/sum.12262

Validation of the ANOCOVA model for regional-scale EC_a to EC_e calibration

D. L. Corwin[1] & S. M. Lesch[2]

[1]*U.S. Salinity Laboratory, USDA-ARS, 450 West Big Springs Road, Riverside, CA 92507-4617, USA, and* [2]*Resource Division, Riverside Public Utilities, 3435 14th St., Riverside, CA 92501, USA*

Abstract

Two approaches have emerged as the preferred means for assessing salinity at regional scale: (i) vegetative indices from satellite imagery (e.g., MODIS enhanced vegetative index, NDVI) and (ii) analysis of covariance (ANOCOVA) calibration of apparent soil electrical conductivity (EC_a) to salinity. The later approach is most recent and least extensively validated. It is the objective of this study to provide extensive validation of the ANOCOVA approach. The validation comprised 77 fields in California's Coachella Valley, ranging from 1.25 to 30.0 ha in size with an average size of 12.8 ha. Mobile electromagnetic induction (EMI) equipment surveyed the fields obtaining geospatial measurements of EC_a. Soil sample sites selected following EC_a-directed soil sampling protocols characterized the range and spatial variation in EC_a across the field. From the data, a regional ANOCOVA model was developed. The regional ANOCOVA model successfully reduced cross-validated, average log salinity prediction error (variance) estimate by more than 30% across the 77 fields and improved the depth-averaged prediction accuracy in 58 of the 77 fields. The results show that the ANOCOVA modelling approach improves soil salinity predictions from EMI signal data in most of the surveys conducted, particularly fields where only a limited number of calibration sampling locations were available. The establishment of ANOCOVA models at each depth increment for a representative set of fields within a regional-scale study area provides slope coefficients applicable to all future fields within the region, significantly reducing ground-truth soil samples at future fields.

Keywords: Salinity mapping, soil spatial variability, electromagnetic induction, proximal sensor, electrical resistivity, regional-scale salinity assessment

Introduction

Characterizing the spatial variability of soil properties, such as salinity, has been and continues to be one of the most significant challenges in soil science. The complex spatial patterns of salinity found on dryland and irrigated agricultural lands make it difficult to map salinity using grid or random sampling because tremendous numbers of samples are necessary. At field scale, apparent soil electrical conductivity (EC_a) directed soil sampling provides the best means of reducing the number of soil samples needed to characterize spatial variability (Corwin & Lesch, 2003, 2005a). Apparent soil EC_a directed soil sampling uses geospatial measurements of EC_a taken with mobile electromagnetic induction (EMI) or electrical resistivity (ER) equipment to serve as a surrogate to characterize the spatial variability of soil salinity or any soil property that correlates with EC_a at the study site (Corwin & Lesch, 2003, 2005a,b, 2013). Intensive geo-referenced EC_a data guide soil sampling in a manner that reflects the spatial variation and range in soil properties correlating with EC_a at a study site. Subsequently, the sample design will spatially characterize the distribution of any soil property that correlates with EC_a for a particular field.

Aside from field-scale salinity assessment, there is a growing need for regional-scale ($10–10^5$ km^2) salinity assessment because of broad-scale salinization of dryland and irrigated agricultural lands resulting from management-induced impacts and climate change. Of the 1.5×10^9 ha of cultivated land, estimates are that about 23% are saline and another 37% are sodic (Massoud, 1981). These estimates and most other more recent estimates of salinization at regional scales are crude at best because they rely on qualitative rather than quantitative approaches for inventorying salinity at large spatial extents. Yet, reliable and accurate regional-

Correspondence: D. L. Corwin. E-mail: Dennis.Corwin@ars.usda.gov
Received February 2015; accepted after revision February 2016

scale maps of the extent of the salinity problem and its rate of change are needed by policy makers to develop strategies and infrastructures (e.g., tile drains and drainage channels) to deal with the problem of salinization.

The Red River Valley (RRV) in the Midwestern USA is a perfect example of the need for regional-scale salinity assessment information. It is the perception of producers in the RRV and of the Natural Resource Conservation Service (NRCS) that management and climate changes have caused water tables to rise and subsequently salinity to increase, but no one knows the extent of the salinity problem in the RRV nor is the rate of salinization known (Lobell *et al*., 2010). Other geographic regions of concern with respect to salinization include northeast China, northern and western India, Pakistan, northeastern Mexico, Middle East, northern and eastern Africa, eastern Australia, and southwestern USA, particularly USA's Coachella, Imperial, and San Joaquin Valleys.

Regional-scale mapping of soil salinity poses new challenges beyond those of field-scale salinity assessment because of the greater spatial extent. Lobell *et al*. (2010) suggested two reasons for the difficulty in mapping soil salinity at large spatial extents. First, 'the high spatial variability of soil salinity limits the ability to interpolate between ground measurements taken at individual points in space.' Second, 'the relative lack of skill of noninvasive, rapid measurement approaches that could provide more continuous spatial monitoring, such as those offered by satellite-based remote sensing instruments.' Lobell *et al*. (2010) and others (e.g., Caccetta *et al*., 2010; Furby *et al*., 2010; Bouaziz *et al*., 2011; Dang *et al*., 2011; Ivits *et al*., 2013) conducted the formative research showing the viability of using vegetative and salinity indices from satellite imagery to map soil salinity at regional scale.

Aside from the use of vegetative indices from satellite imagery to map soil salinity at regional scale, such as the MODIS enhanced vegetative index and normalized difference vegetation index (Lobell *et al*., 2010), another approach has recently emerged, that is, the use of analysis of covariance (ANOCOVA) to calibrate EC_a to salinity over large spatial extents (i.e., hundred thousand hectares). Harvey & Morgan (2009) and Corwin & Lesch (2014) showed that a calibration of EC_a to salinity over large spatial extents is possible using ANOCOVA regression models. Corwin & Lesch (2014) observed that abrupt changes in the magnitude of EC_a occurred across field boundaries in multi-field surveys. This presents a challenge to the conversion of EC_a to salinity when mapping across thousands to tens of thousands of hectares. The ANOCOVA calibration models adjust out any abrupt change (Corwin & Lesch, 2014). Of the two approaches (i.e., vegetative indices from satellite imagery and ANOCOVA calibration), the latter is the least extensively validated. It is the objective of this study to validate the ANOCOVA regression modelling technique for calibrating EC_a to salinity (i.e., electrical conductivity of the saturation extract, EC_e; dS/m) for a far more extensive dataset (i.e., 77 fields) than previous validations.

Materials and methods

The ANOCOVA modelling technique for regional-scale EC_a – EC_e calibration was evaluated using an extensive spatial dataset obtained for California's Coachella Valley.

Study area

Coachella Valley is a desert valley in Southern California that extends 72 km from the San Bernardino Mountains southeast to the northern shore of the Salton Sea with a width of approximately 24 km. It is extremely arid with most of the precipitation falling during the winter months and temperatures ranging from 8 to 44 °C. Approximately 40 500 ha of land is irrigated producing a wide range of fruits and vegetables including table grapes, citrus fruits (e.g., lemons, limes, oranges and grapefruit), mangoes, nectarines, peaches, plums, strawberries, lettuce, onions, leeks, potatoes, radishes, spinach tomatoes, peppers, artichokes, beans, avocados, beets, cabbage, carrots, corn, cucumbers, eggplant, figs, dates, as well as grains (e.g., barley, oats, rye, and wheat) and cotton, with an estimated value of USD $600 million. All of the fields selected in the study were agricultural land. The fields in the study fell into the following six soil series: Carsitas, Coachella, Gilman, Indio, Myoma and Salton. With 80% of the acreage of the fields selected for study categorized as either Gilman or Indio. All of the soils in the study area are coarse-textured soils classified as Entisols, which are soils that show little or no evidence of development of differing horizons or layers. In the Coachella Valley area, there are three major sources of parent material: (i) recent outwash, which is mainly granitic material from the mountains surrounding the Coachella Valley; (ii) lacustrine deposits of Lake Cahuilla; and (iii) the weathered rock in the San Jacinto Mountains.

Dataset

The dataset consisted of EMI measurements of EC_a and associated soil sample information for 82 fields. Surveying and soil sampling of all 82 fields occurred between 2002 and 2008, with the majority performed on or after January 2005. The EMI survey information was initially examined for internal consistency and reliability, that is, properly correlated and aligned EMI readings that were all positive and devoid of gross outliers, systematic instrument bias, and any obvious calibration error effects. Out of the 82 field sites, 80 sites passed all internal consistency and reliability tests.

The data associated with the remaining 80 field sites were each assessed using the dynamic Dual Pathway Parallel Conductance (dynamic DPPC) correlation analysis of Lesch & Corwin (2003). In these analyses, the calculated EC_a readings (as computed from measured soil salinity, saturation percentage or SP, and gravimetric water content measurements) were compared with the average of the EMI signal data on a log–log basis, after adjusting for potentially low water content levels. An a priori threshold correlation level of 0.5 was specified as the minimum acceptable correlation level for identifying reliable survey data. Of the 80 fields, 77 fields produced dynamic DPPC correlation levels greater than 0.5; consequently, these 77 field sites were chosen to comprise the validation database for EC_a – EC_e calibration.

Electromagnetic induction (EMI) EC_a surveys

Geospatial EC_a measurements were taken at each field site with EMI using a Geonics EM38 EC_a meter[1]. Protocols and guidelines that ultimately resulted in the EC_a-directed soil sampling methodology papers by Corwin & Lesch (2003, 2005b, 2013) were followed. The surveys consisted of geospatial EC_a measurements taken with mobile EMI equipment. Electromagnetic induction measurements of EC_a were obtained in the horizontal (EM_h) and vertical coil configurations (EM_v). The EM_h and EM_v measurements provide a shallow (i.e., depth of penetration 0.5–0.75 m) and deep (i.e., depth of penetration 1.0–1.5 m) measurement of EC_a, respectively. This information provides an indication if the salinity profile is uniform (EM_h EC_a = EM_v EC_a), inverted (EM_h EC_a > EM_v EC_a) or regular (EM_h EC_a < EM_v EC_a). The characterization of spatial variability of EC_a is often enhanced by the inclusion of both EM_h and EM_v measurements in the sample site selection (Corwin & Lesch, 2003).

Table 1 shows the general field-size and EMI survey statistics for the 77 field sites. The table quantifies the distribution of field sizes and the number of EMI measurement locations recorded in each field. The average field size was approximately 12.8 ha; 50% of the fields were between 8.1 and 15.8 ha and the smallest and largest fields were 1.3 and 30.1 ha, respectively. The average number of EMI survey positions was about 1550 and the survey data associated with 50% of the fields contained 1254 to 1795 locations.

Soil sampling

Within each field, the selected soil sample locations reflected the range and variation in EC_a. To achieve this, the model-based sampling strategy in the ESAP software package selected the calibration sampling locations (Lesch *et al.*, 2000). The model-based sampling strategy is a response surface sampling design (RSSD). The RSSD creates a 3-D surface of the EC_a measurements. Based on the range and variation in EC_a, RSSD selects locations that characterize the variation in EC_a while maximizing the distances between adjacent sampling locations.

Either 6 or 12 sampling locations were identified in each field. Table 2 shows the number of 6- and 12-site soil sampling plans for the 77 fields. The majority of fields (i.e., 60 fields) were sampled using a six-site ESAP sampling plan. The remaining 17 fields were sampled using a 12-site plan, although four of these fields contained either 10 or 11 sampling sites. Overall, the validation soil sample database contains $N = 6(60) + 10(1) + 11(3) + 12(13) = 556$ sampling locations across 77 fields.

Soil samples were collected at 30-cm depth increments. Not all fields were sampled to the same depth. The validation soil database consisted of 77, 59 and 15 fields sampled to depths of 60, 90 and 120 cm, respectively.

Using the method presented in Rhoades (1996), a saturation extract of each soil sample was prepared and the EC_e (dS/m) was measured. Saturation percentage and water content were determined gravimetrically.

General characteristics of field sites

Figure 1 identifies the locations of the 77 field sites based on the Universal Transverse Mercator (UTM) coordinate system. The 77 field sites are located within a 30 km by 30 km area within California's Coachella Valley. Overall, the coverage across the valley is comprehensive, particularly given the non-random manner in which the fields were selected, which was largely dependent on the willingness of

Table 1 General summary statistics for the 77 validated field studies

	Field information	
Statistic	Size (ha)	No. of EMI sites
Mean	12.8	1550.3
Standard deviation	5.6	689.4
Skewness	0.0	1.8
Quantiles:		
Minimum	1.3	404
10%	4.9	735
25%	8.1	1254
Median (50%)	14.5	1429
75%	15.8	1795
90%	19.0	2487
Maximum	30.1	4998

EMI, electromagnetic induction.

[1]Geonics, Mississaugua, Ontario, Canada. Product identification does not imply endorsement by USDA.

Table 2 Sample design and sampling depths for the 77 validated fields: (a) number of ESAP-generated sampling sites for each field and (b) number of sampling depths for each field

	Number of fields	Remarks
(a) Soil sampling design		
6-site design	60	
12-site design	17	Three fields were sampled at 11 locations, one field at 10 locations
(b) Depth increments		
2	23	5 of 23 fields sampled in 60 cm depth increments
3	44	All 44 fields sampled in 30 cm depth increments
4	10	All 10 fields sampled in 30 cm depth increments

ESAP, EC_e Sampling, Assessment, and Prediction Software.

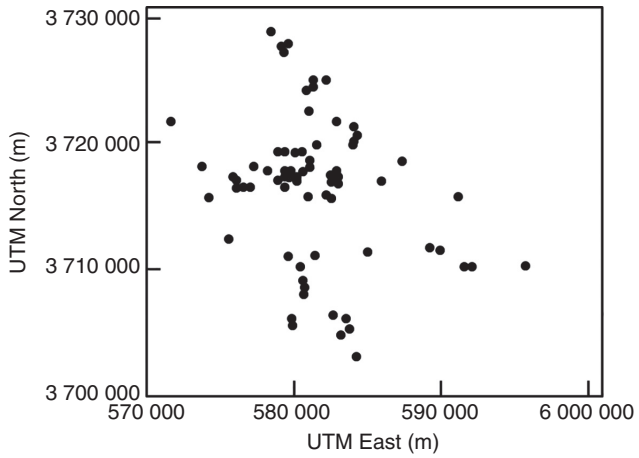

Figure 1 Universal Transverse Mercator (UTM) locations of the 77 field sites in California's Coachella Valley.

landowners to participate in the study. The 77 field sites provided an extremely challenging and rigorous evaluation of the regression techniques by testing sites scattered over several hundred thousand hectares with wide ranging differences in areal extent, soil properties, bed-furrow surface geometry, crop and irrigation management, and geographic location, each of which can influence the EC_a to EC_e calibration (Corwin & Lesch, 2003, 2005b).

Table 3 indicates the number of fields exhibiting soil sample data with adequate (>70%), marginal (50–70%), and excessively dry (<50%) average water content relative to field capacity (WCFC). As pointed out by Corwin & Lesch (2013), a WCFC of <50% may cause spurious EC_a measurements because of the disruption of electrical conductance through the liquid pathway. Table 3 indicates

Table 3 Calculated water content classes relative to estimated field capacity by depth increment

Depth increment	WCFC class	Number of fields
1st Increment	>70%	37
	50–70%	28
	<50%	12
2nd Increment	>70%	50
	50–70%	14
	<50%	13
3rd Increment	>70%	33
(Note: 23 fields are missing	50–70%	10
the 3rd depth increment)	<50%	11

WCFC, average water content relative to field capacity in percentage of field capacity.

that 11–13 fields in the database appear to have been sampled under excessively dry conditions (i.e., WCFC Class <50%); at least five of these fields (Fields #1, #6, #15, #32, and #49) show marked differences between their ordinary and dynamic DPPC correlation coefficients (Figure 2).

Table 4 quantifies the land cover associated with various NRCS classified soil series. All of the soil series except Salton were classified as either fine sands or fine sandy loams (Salton Sb is classified as silty clay loam). The predominant soil order is Entisols.

Statistical methodology: model definitions and statistical assumptions

Three linear regression models were used for predicting the natural log transformed soil salinity from natural log transformed EM38 signal readings. The regression techniques include field specific regression (FSR), common coefficient regression (CCR), and ANOCOVA. Equation (1) defines a FSR model:

$$\ln(EC_{e,ijk}) = \beta_{0,jk} + \beta_{1,jk}\ln(EM_{v,ik}) + \beta_{2,jk}\ln(EM_{h,ik}) + \varepsilon_{ijk} \quad (1)$$

Equation (2) defines a CCR model:

$$\ln(EC_{e,ijk}) = \beta_{0,j} + \beta_{1,j}\ln(EM_{v,ik}) + \beta_{2,j}\ln(EM_{h,ik}) + \varepsilon_{ijk} \quad (2)$$

Equation (3) defines an ANOCOVA model:

$$\ln(EC_{e,ijk}) = \beta_{0,jk} + \beta_{1,j}\ln(EM_{v,ik}) + \beta_{2,j}\ln(EM_{h,ik}) + \varepsilon_{ijk} \quad (3)$$

where i refers to the soil sample site within a field (i = 1, 2, 3, … , n_k), j is the sample depth (j = 1, 2, 3, … , p), k is the field (k = 1, 2, 3, … , M), EM_v is the EC_a measured with EMI in the vertical coil configuration (dS/m), and EM_h is the EC_a measured with EMI in the horizontal coil configuration (dS/m).

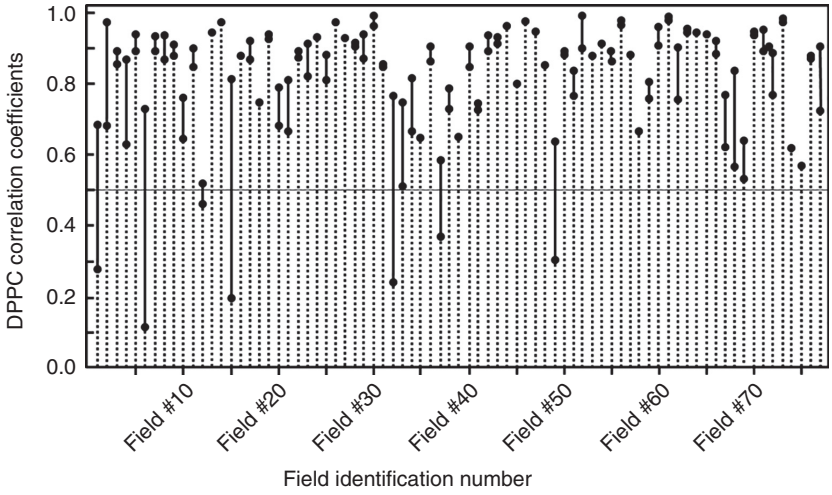

Figure 2 Ordinary (dashed line) and dynamic (solid line) Dual Pathway Parallel Conductance (DPPC) correlation coefficients for the 77 field sties.

Table 4 Land cover of associated soil series for 76 of 77 field sites in the Coachella Valley. One surveyed field without any associated soil-type information was excluded from this table

Soil series	Symbol	Hectares	% of Total land cover
Carsitas	CdC	26.5	3.07
	CkB	3.1	0.36
Coachella	CpA	4.4	0.51
	CpB	7.3	0.85
	CrA	55.2	6.38
Gilman	GaB	4.65	0.54
	GbA	37.1	4.29
	GcA	222.1	25.69
	GdA	1.8	0.21
	GfA	50.7	5.87
Indio	Ip	2.1	0.24
	Ir	69.6	8.05
	It	294.6	34.09
Myoma	MaB	23.4	2.71
	McB	18.0	2.08
Salton	Sb	43.9	5.07

All three coefficients of FSR model equation (1) change across fields and sampling depths; that is, all of the regression model coefficients need to be re-estimated whenever a new field is surveyed. In contrast, the EM38 slope coefficients in ANOCOVA model equation (3) only change across sampling depths, but not across fields. Only the intercept coefficients change across fields and sampling depths in the ANOCOVA model. The coefficients do not change across fields in CCR model equation (2); these coefficients can only change across sampling depths.

There are well-established reasons why the FSR model should be the most accurate regression-based calibration equation (Lesch & Corwin, 2003). However, the FSR model can be difficult to estimate accurately when only a small number of calibration soil samples are available for a given field. Additionally, many of the field-specific effects on EM38 survey data such as seasonal changes in soil temperature, bed-furrow geometry, surface roughness and instrument placement height are multiplicative. Therefore, on the log-transformed scale these effects become additive constants, which in theory should only affect the intercept coefficient. Thus, there are legitimate theoretical and statistical reasons to expect that the ANOCOVA model might actually perform better than the FSR model, particularly when only limited calibration data are available and the EM38 survey data are acquired over a short time span (i.e., over a period of hours within any specific field).

Assuming that a total of M fields have been surveyed, the FSR model requires $3M$ parameter estimates to produce soil salinity predictions across all M fields for a specified sampling depth. In contrast, for a specific sampling depth the ANOCOVA model requires only $M + 2$ parameter estimates (or just M estimates, if the EM38 slope coefficients have already been established). Of course, the CCR model requires only three parameter estimates, but in general, this model will not be very accurate. The CCR model has been included in this study primarily as a baseline reference model, rather than a formal prediction model.

In the following analyses, the residual errors associated with both the FSR and ANOCOVA models are assumed to be normally distributed, independent across fields, and spatially uncorrelated within a field. The first two assumptions are typically reasonable, while the third assumption is generally met when model-directed sampling strategies are used to select the calibration sample locations, as is the case for the spatial response surface sampling strategy used by ESAP software. Additionally, the errors are assumed to be correlated across sampling depths at the same site and the error variances are assumed to change across fields (and sometimes across sampling depths). Under these

residual error assumptions, either ordinary or mixed linear modelling techniques can be used to estimate the parameter coefficients in either the FSR or ANOCOVA models.

Statistical evaluation of prediction error

The prediction accuracy of the three regression techniques was evaluated by a comparison of their jack-knifed mean square prediction error (MSPE) shown in equation (4):

$$\mathrm{MSPE} = \frac{1}{N_{ijk}} \sum_{i,j,k} \left(y_{ijk} - \hat{y}_{ijk,(-i)}\right)^2 \qquad (4)$$

where $y_{ijk} = \ln(EC_{e,ijk})$ and $\hat{y}_{ijk,(-i)}$ represents the model predicted $\ln(EC_{e,ijk})$ where the i^{th} observed natural log salinity measurement has not been used to calibrate the regression equation and N_{ijk} represents the total number of jack-knifed soil salinity samples. Along with the computation of various MSPE estimates, a detailed analysis of the ANOCOVA model residuals was conducted. The residual assessment analysis was performed to verify that the previously discussed modelling assumptions are reasonable.

Results and discussion

Soil salinity (EC_e) and EM38 apparent soil EC_a data

Table 5 shows the EC_e and co-located EM38 EC_a univariate summary statistics for the pooled dataset comprised of the 77 fields. The majority of the EC_e measurements are low. The median salinity levels are less than 3 dS/m across all four sampling depth increments and at least 25% of the EC_es are less than 1.2 dS/m. However, approximately 10% of the EC_es from each depth increment are greater than 10 dS/m. The pooled salinity distributions are strongly right skewed, indicating that EC_e values are log normally distributed. The EM38 EC_a signal readings for EM_h and EM_v exhibit similar characteristics.

The correlation coefficients between the log transformed EC_e and EM38 readings are moderate to high. The correlation coefficients between $\ln(EC_e)$ and $\ln(EM_h)$ are 0.668, 0.801, 0.751 and 0.802 for the depth increments 0–30, 30–60, 60–90 and 90–120 cm, respectively. The correlation coefficients between $\ln(EC_e)$ and $\ln(EM_v)$ are 0.618, 0.773, 0.756 and 0.785 for the depth increments 0–30, 30–60, 60–90 and 90–120 cm, respectively. All coefficients are statistically significant below the 0.0001 level. The results indicate that the EM38 data predicts the soil salinity levels provided adequate models could be derived that suitably adjust for different secondary characteristics across fields.

A more detailed assessment of the EC_e – EM38 EC_a correlation structure is obtained by calculating the ordinary and dynamic DPPC correlation coefficients for each field as described by Lesch & Corwin (2003). Summary statistics concerning these coefficients are in Table 6. Recall that fields exhibiting dynamic DPPC coefficients less than 0.5 were removed from the final database; hence, all 77 dynamic DPPC coefficients are obviously greater than 0.5. The average dynamic DPPC correlation value in the database is 0.858 and 75% of the fields produce correlation coefficients greater than 0.8, suggesting that the majority of the survey data exhibit a high degree of internal consistency and reliability. The ordinary DPPC correlation coefficients are somewhat lower (average value = 0.777; 75% of the fields exhibit correlation coefficients greater than 0.66). These generally lower ordinary DPPC coefficients suggest that the EM38 signal data in at least some of the 77 field surveys were moderately influenced by low field water content conditions. The DPPC correlation plot in Figure 2 confirms the notion that low water content conditions influenced some of the field surveys. Figure 2 shows that there are seven fields (Fields #1, #6, #12, #15, #32, #37, and #49) that exhibit abnormally low ordinary DPPC correlation coefficients (i.e., <0.5). In addition, 10 fields (Fields #1, #2, #4, #6, #15, #32, #33, #37, #49, and #68) exhibit dynamic DPPC correlation coefficients that are at least 0.2 units greater than their corresponding ordinary DPPC coefficients. Hence, there appears to be a

Table 5 Soil salinity (EC_e) and co-located EMI EC_a (EM_h and EM_v) summary statistics for four depth increments of 77 fields in Coachella Valley, CA

	Salinity (EC_e, dS/m) by depth increment				EC_a (mS/m)	
Statistic	0–30 cm	30–60 cm	60–90 cm	90–120 cm	EM_h	EM_v
N	559	559	450	106	559	559
Mean	5.06	4.77	4.47	4.63	73.42	95.73
Standard deviation	9.05	8.81	6.65	5.65	91.90	107.94
Skewness	4.34	4.23	5.21	2.40	3.03	2.92
Quantiles:						
Minimum	0.12	0.10	0.10	0.19	8.50	10.88
5%	0.58	0.44	0.56	0.42	14.75	21.88
10%	0.72	0.56	0.71	0.72	17.50	27.88
25%	1.04	0.84	1.10	1.14	24.25	38.00
Median (50%)	2.11	1.80	2.12	2.90	39.38	57.88
75%	4.48	4.20	5.00	5.47	76.00	99.88
90%	12.60	11.62	10.65	9.60	179.25	223.13
95%	20.10	19.61	16.80	20.60	267.38	341.50
Maximum	66.70	72.60	83.50	27.40	658.88	718.25

N, number of soil samples or EM38 measurements; EMI, electromagnetic induction; EC_e, electrical conductivity of the saturation extract (dS/m); EC_a, apparent soil electrical conductivity (dS/m); EM_h, apparent soil electrical conductivity measured by EM38 in the horizontal configuration; EM_v, apparent soil electrical conductivity measured by EM38 in the vertical configuration.

stronger than normal water content influence on the EM38 signal data in at least 10 of the 77 fields.

Prediction accuracy (MSPE statistics)

Table 7 presents the FSR, ANOCOVA and CCR model summary statistics pertaining to the models for the 0–30, 30–60 and 60–90 cm sampling depth increments. No model was fit to the 90–120 cm depth increment because of the limited number of fields containing soil sample data at that depth increment. The R^2 and mean square error (MSE) estimates shown in Table 7 for the FSR models represent composite statistics, that is, composite estimates calculated by pooling all of the individual fields together. The R^2 and MSE estimates corresponding to the ANOCOVA models were computed using ordinary least squares (OLS) estimation, which assumes a homogeneous residual variance component across fields. The ANOCOVA model R^2 values are about 9–10% smaller than the FSR model R^2 values. The ANOCOVA MSE estimates are about 0.05–0.06 units larger. In contrast, the CCR model R^2 values are noticeably smaller than both the ANOCOVA and FSR model R^2 values and the CCR MSE estimates are clearly much larger.

The overall average and depth-specific MSPE estimates associated with the FSR, ANOCOVA, and CCR models are in Table 8. Unlike the model summary statistics of Table 7 that essentially measure how well each model 'fits' the sample data, the MSPE values in Table 8 provide a more reliable estimate of the prediction accuracy associated with each model. All of the MSPE estimates associated with the ANOCOVA models are considerably smaller than either the FSR or CCR estimates. When compared with the depth-specific FSR estimates, the ANOCOVA MSPE is about 30% smaller for the 0–30 cm depth increment, 29% less for the 30–60 cm depth increment, and 41% smaller for the 60–90 depth increment. Likewise, the overall average ANOCOVA MSPE estimate is roughly 33% less than both the FSR and CCR MSPE estimates. These results indicate that the ANOCOVA models produce the most accurate log salinity predictions, that is, the jack-knifed variance of the prediction errors associated with the ANOCOVA model is only about 2/3 as large as the jack-knifed variance of the FSR model prediction errors.

Overall, ANOCOVA models more accurately predicted the jack-knifed salinity patterns in 58 out of 77 fields (75%). For fields with only six soil sample sites, the percentage increased slightly (47 out of 60 or approximately 78%). For fields having 10–12 sample sites, the percentage was somewhat lower (11 of 17 or approximately 65%). As the number of calibration samples increases, the FSR model would be expected to out-perform the ANOCOVA model. However, the results suggest that the prediction accuracy in more than half of the fields associated with a 12-site ESAP sampling plan can still be improved using the ANOCOVA modelling approach. The prediction accuracy in about 80% of the

Table 6 Summary statistics for the field-specific ordinary and dynamic DPPC (Dual Pathway Parallel Conductance) correlation coefficients

	Correlation coefficients	
Statistic	Ordinary DPPC	Dynamic DPPC
Mean	0.777	0.858
Standard deviation	0.200	0.114
Skewness	−1.51	−1.14
Quantiles:		
Minimum	0.117	0.521
10%	0.515	0.653
25%	0.669	0.801
Median (50%)	0.866	0.894
75%	0.911	0.940
90%	0.964	0.977
Maximum	0.986	0.992

Table 7 Comparison of FSR (Field Specific Regression), ANOCOVA (Analysis of Covariance), and CCR (Common Coefficient Regression) model summary statistics (i.e., R^2 and mean square error, MSE) for three depth increments of 77 fields in Coachella Valley, CA

		Depth increment (cm)		
Model	Statistic	0–30	30–60	60–90
FSR	R^2	0.886	0.890	0.837
	MSE	0.241	0.266	0.304
ANOCOVA	R^2	0.792	0.803	0.733
	MSE	0.302	0.326	0.349
CCR	R^2	0.460	0.642	0.578
	MSE	0.675	0.512	0.481

Table 8 Comparison of FSR (Field Specific Regression), ANOCOVA (Analysis of Covariance), and CCR (Common Coefficient Regression) jack-knifed prediction statistic (i.e., mean square prediction error, MSPE) for three depth increments of 77 fields in Coachella Valley, CA

	Mean square prediction error (MSPE)			
		Depth increment (cm)		
Model	Pooled average	0–30	30–60	60–90
FSR	0.564	0.499	0.535	0.681
ANOCOVA	0.376	0.350	0.379	0.404
CCR	0.565	0.680	0.515	0.485

Table 9 Distribution of ANOCOVA jack-knifed mean square prediction error (MSPE) estimates for 0–0.90 m depth of 77 fields in Coachella Valley, CA

MSPE range	Grade	Prediction accuracy	Number of fields	% of Total sample size	Correlation of observed and predicted salinity
<0.15	A	Excellent	16	21	0.921
0.15–0.30	B	Good	23	30	0.860
0.30–0.60	C	Fair	24	31	0.795
0.4					
>0.60	U	Unacceptable	14	18	0.693

ANOCOVA, analysis of covariance.

fields associated with a reduced six-site plan improved using the ANOCOVA modelling approach.

Evaluation of the reliability of the salinity predictions from the ANOCOVA approach consisted of 'grading' the predictions into four MSPE classes: excellent (grade A; MSPE <0.15), good (grade B, $0.15 \leq \text{MSPE} \leq 0.30$), fair (grade C; $0.30 < \text{MSPE} \leq 0.60$), and unacceptable (grade U; MSPE >0.60). Table 9 shows the distribution of the ANOCOVA model jack-knifed MSPE into the four classes. Approximately, 82% of the fields (63 of 77) exhibit either excellent (grade A), good (grade B) or fair (grade C) prediction reliability with corresponding correlation coefficients of the observed and predicted salinity of 0.921 (excellent; grade A), 0.860 (good; grade B) and 0.795 (fair; grade C). Mean square prediction errors less than 0.6 suggest that the salinity levels in a particular field are well-described (i.e., strongly correlated with) by the associated EM38 survey data; 14 of the 77 fields fall into this 'unacceptable' class. Figure 3a–d graphically shows the observed versus jack-knife predicted salinities for the groups of fields exhibiting A (excellent), B (good), C (fair) and U (unacceptable) prediction accuracy grades, respectively.

ANOCOVA model: residual analysis and diagnostic statistics

As mentioned previously the residual errors associated with the ANOCOVA were assumed to be normally distributed, independent across fields and spatially uncorrelated within a field. When ANOCOVA models are estimated using OLS techniques, it is assumed that the residual variance does not change across fields. However, this last assumption often times does not hold, and thus must be assessed.

A summary of the ANOCOVA model residual errors is presented in Table 10. The upper portion of Table 10 lists the global residual variance estimates for the three sampling depth increments, in addition to the pooled residual correlation matrix. All of the off-diagonal correlation

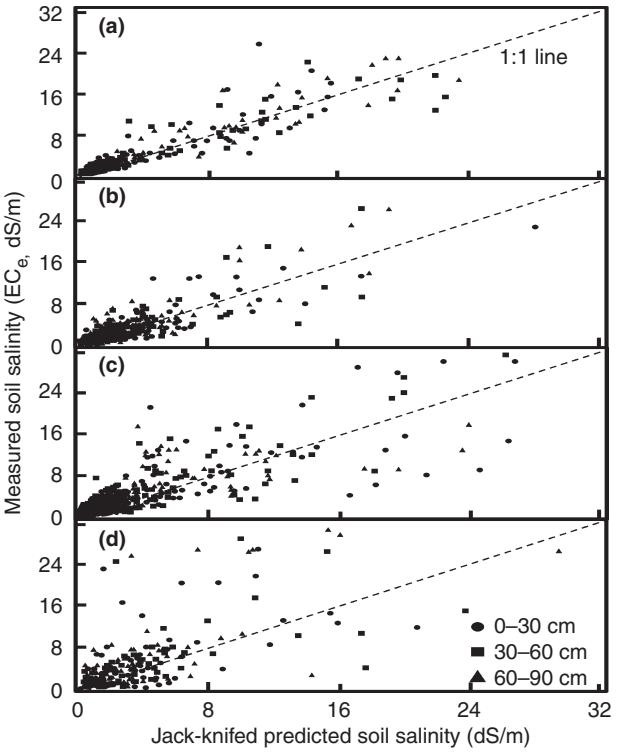

Figure 3 Measured versus jack-knifed predicted soil salinity (EC_e, dS/m) at depth increments of 0–30, 30–60 and 60–90 cm for fields with mean square predictions errors (MSPE) (a) <0.15 (grade A, excellent), (b) 0.15–0.30 (grade B, good), (c) 0.30–0.60 (grade C, fair) and (d) >0.60 (grade U, unacceptable).

coefficients are positive and statistically different from zero ($P < 0.0001$), confirming that the ANOCOVA model residual errors associated with the specific sampling locations are indeed correlated across sampling depths. This does not invalidate the OLS estimation techniques since unique ANOCOVA models have been fit to each depth.

The center portion of Table 10 lists the test results and *P*-values for the Shapiro-Wilk Normality goodness-of-fit (GOF) test. The pooled set of ordinary residuals from the three ANOCOVA models clearly fails this test ($P < 0.0001$). The associated residual quantile plot (Figure 4) suggests that the residual distribution is somewhat 'heavy tailed.' Figure 5 displays the residual variance pattern across the 77 surveyed fields. Figure 5 shows that the degree of residual variation is field dependent. However, after standardizing the pooled set of residuals by their individual field variance estimates, the new variance-standardized residuals pass the Shapiro–Wilk GOF test ($P = 0.540$).

Overall, the residual diagnostic results suggest that the ANOCOVA model errors do follow a normal distribution, but the variance of the distribution changes across the 77 fields. The lower portion of Table 10 shows the formal Chi-square test results for the non-constant residual variance hypothesis (i.e., the likelihood ratio tests associated with the

Table 10 ANOCOVA model residual errors; depth-increment correlation structure and pooled residual distribution assessments

		Residual correlation matrix			
Depth increment	Residual variance	Depth increment	0–30 cm	30–60 cm	60–90 cm
0–30 cm	0.302	0–30 cm	1.00	0.48	0.21
30–60 cm	0.326	30–60 cm	0.48	1.00	0.49
60–90 cm	0.349	60–90 cm	0.21	0.49	1.00

Shapiro–Wilks normality tests: polled residuals (N = 1568)

Residuals:	W-score	*P*-value
Ordinary residuals	0.9867	<0.0001
Variance standardized residuals (by field)	0.9990	0.5400

Depth-specific χ^2 tests for non-constant residual variance across fields

Depth increment & model:	χ^2-score	Degrees of freedom	*P*-value
0–30 cm ANOCOVA model	188.9	76	<0.0001
30–60 cm ANOCOVA model	144.4	76	<0.0001
60–90 cm ANOCOVA model	139.6	58	<0.0001

ANOCOVA, analysis of covariance.

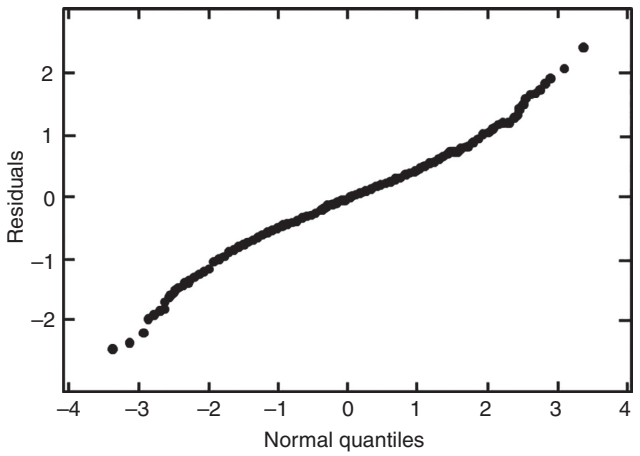

Figure 4 Residual QQ plot of ordinary analysis of covariance (ANOCOVA) model residuals.

mixed linear ANOCOVA models estimated using restricted maximum likelihood). The test results for all three ANOCOVA models are highly significant ($P < 0.0001$) indicating that these heterogeneous variance ANOCOVA models should be used to produce the final set of $\ln(EM_v)$ and $\ln(EM_h)$ parameter coefficients.

Table 11 shows the calculated ANOCOVA model $\ln(EM_v)$ and $\ln(EM_h)$ parameter coefficients for models estimated under homogeneous (common) and heterogeneous (field specific) variance assumptions. The estimated standard errors of the coefficients are in parentheses. The standard errors confirm that the model coefficients associated with the heterogeneous variance (mixed linear) ANOCOVA models are more accurately estimated and should be the coefficients that are used to calibrate EC_a to EC_e in the Coachella Valley when the ANOCOVA modelling approach is used.

Substituting the depth-specific EM38 parameter coefficients shown in Table 11 into the ANOCOVA model of equation (3) results in equations (5)–(7) for the depth increments 0–30, 30–60 and 60–90 cm, respectively:

$$\ln(EC_{e,0-30,i}) = \hat{\beta}_{0,0-30} - 0.413\ln(EM_{v,i}) + 1.178\ln(EM_{h,i}) + \varepsilon_{0-30,i} \quad (5)$$

$$\ln(EC_{e,30-60,i}) = \hat{\beta}_{0,30-60} + 0.150\ln(EM_{v,i}) + 1.080\ln(EM_{h,i}) + \varepsilon_{30-60,i} \quad (6)$$

$$\ln(EC_{e,60-90,i}) = \hat{\beta}_{0,60-90} + 0.976\ln(EM_{v,i}) + 1.129\ln(EM_{h,i}) + \varepsilon_{60-90,i} \quad (7)$$

where the subscript $i = 1, 2, \ldots, N$ refers to the i^{th} sampling location in a given field. Equations (5)–(7) are used to compute the depth-specific intercept estimates (i.e., $\hat{\beta}_{0,0-30}$, $\hat{\beta}_{0,30-60}$, and $\hat{\beta}_{0,60-90}$) and the corresponding pooled MSPE estimate, which represents a measurement of how well the ANOCOVA model fits the data. The intercept estimates are simply the average values of the differenced natural log salinity – natural log EM38 readings:

$$\hat{\beta}_{0,0-30} = \left(\frac{1}{n}\right)\sum_{i=1}^{n}\left[\ln(EC_{e,0-30,i}) + 0.413\ln(EM_{v,i}) - 1.178\ln(EM_{h,i})\right] \quad (8)$$

$$\hat{\beta}_{0,30-60} = \left(\frac{1}{n}\right)\sum_{i=1}^{n}\left[\ln(EC_{e,30-60,i}) - 0.150\ln(EM_{v,i}) - 1.080\ln(EM_{h,i})\right] \quad (9)$$

$$\hat{\beta}_{0,60-90} = \left(\frac{1}{n}\right)\sum_{i=1}^{n}\left[\ln(EC_{e,60-90,i}) - 0.976\ln(EM_{v,i}) - 1.129\ln(EM_{h,i})\right] \quad (10)$$

where n represents the number of sampling locations in the field. Once the intercepts have been obtained, the depth-specific MSPE estimates can then be calculated as

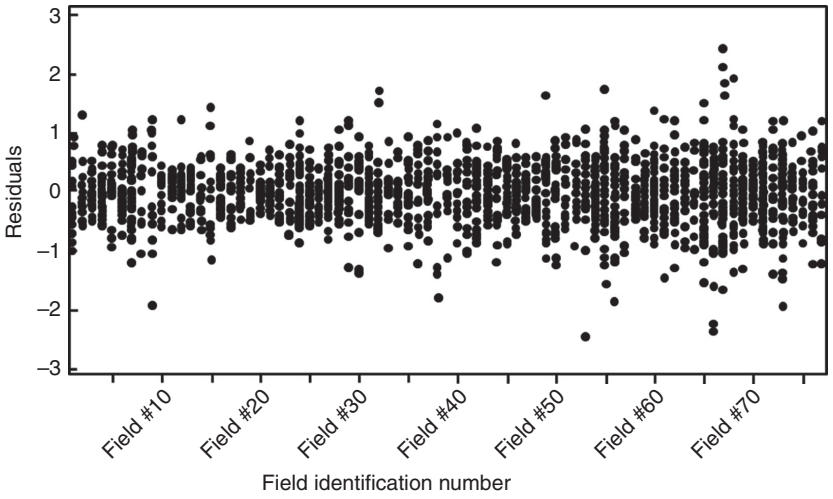

Figure 5 Analysis of covariance (ANOCOVA) residual variance plot, stratified by field.

Table 11 Calculated ANOCOVA model $\ln(EM_v)$ and $\ln(EM_h)$ parameter coefficients for models estimated under homogeneous (common) and heterogeneous (field specific) variance assumptions. Estimated standard errors of the parameter coefficients are in parentheses

	Common variance assumption		Field-specific variance assumption	
Depth Increment (cm)	$\ln(EM_v)$	$\ln(EM_h)$	$\ln(EM_v)$	$\ln(EM_h)$
0–30	−0.696 (0.170)	1.557 (0.159)	−0.413 (0.128)	1.178 (0.117)
30–60	0.114 (0.177)	1.219 (0.165)	0.150 (0.127)	1.080 (0.119)
60–90	0.833 (0.191)	0.317 (0.178)	0.976 (0.123)	0.129 (0.117)

ANOCOVA, analysis of covariance; EM_h, apparent soil electrical conductivity measured with electromagnetic induction in the horizontal coil configuration (dS/m); EM_v, apparent soil electrical conductivity measured with electromagnetic induction in the vertical coil configuration (dS/m).

$$\hat{\sigma}^2_{0-30} = \left(\frac{1}{(n-1)}\right)\sum_{i=1}^{n}\left(x_{0-30,i} - \hat{\beta}_{0,0-30,i}\right)^2 \qquad (11)$$

$$\hat{\sigma}^2_{30-60} = \left(\frac{1}{(n-1)}\right)\sum_{i=1}^{n}\left(x_{30-60,i} - \hat{\beta}_{0,30-60,i}\right)^2 \qquad (12)$$

$$\hat{\sigma}^2_{60-90} = \left(\frac{1}{(n-1)}\right)\sum_{i=1}^{n}\left(x_{60-90,i} - \hat{\beta}_{0,60-90,i}\right)^2 \qquad (13)$$

where $x_{0-30,i} = \ln(EC_{0-30,i}) + 0.413\ln(EM_{v,i}) - 1.178\ln(EM_{h,i})$, $x_{30-60,i} = \ln(EC_{30-60,i}) - 0.150\ln(EM_{v,i}) - 1.080\ln(EM_{h,i})$, and $x_{60-90,i} = \ln(EC_{60-90,i}) - 0.976\ln(EM_{v,i}) - 0.129\ln(EM_{h,i})$. The pooled MSPE is calculated by simply averaging the depth-specific MSPE estimates [i.e., equations (11)–(13)], which are then used to 'grade' (i.e., grade A, B, C and U; see Table 9) the overall prediction reliability. The ANOCOVA parameter estimation technique is equivalent to calculating the means and variances of the differenced natural log salinity and natural log EM38 data (i.e., $x_{0-30,i}$, $x_{30-60,i}$ and $x_{60-90,i}$).

Table 12 shows a set of ANOCOVA parameter estimations for Field #47 from the database of 77 fields. The intercepts are $\hat{\beta}_{0,0-30} = -1.659$, $\hat{\beta}_{0,0-30} = -3.383$ and $\hat{\beta}_{0,0-30} = -2.993$ and the pooled MSPE is 0.127. The pooled MSPE is less than 0.15; consequently, the prediction accuracy is excellent, causing a high level of confidence in the corresponding ANOCOVA model salinity predictions.

Figure 6 shows the ESAP generated EM_v map for Field #47 (Figure 6a) and the corresponding 0–90 cm average EC_e map (Figure 6b). The field-wide average 0–90 cm salinity level for Field #47 is 2.06 dS/m and 90% of the individual predictions fall between 1.55 and 2.78 dS/m. Figure 6 shows that Field #47 is primarily non-saline, with some slightly saline areas (i.e., EC_e >3 dS/m) located in a couple of small pockets in the northeast quarter of the field. Based strictly on salinity level, all moderately salt-sensitive (i.e., salinity threshold of 1.5–3 dS/m) to salt tolerant (i.e., salinity threshold of 6–10 dS/m) crops will produce 100% yields over the entire field. Only very small areas in the northeast corner (areas with EC_e >3 dS/m)

Table 12 Analysis of covariance (ANOCOVA) model calculations of intercept estimates ($\hat{\beta}_{0,0-30}$, $\hat{\beta}_{0,30-60}$, and $\hat{\beta}_{0,60-90}$) and mean square prediction error estimates ($\hat{\sigma}^2_{0-30}$, $\hat{\sigma}^2_{30-60}$ and $\hat{\sigma}^2_{60-90}$) for Field #47. MSPE is the mean square prediction error

Depth increment (cm)	Sample site ID#	Salinity (EC_e; dS/m)	EM_v (mS/m)	EM_h (mS/m)	Differenced natural log salinity and natural log EM38 data ($x_{0-30,i}$, $x_{30-60,i}$, or $x_{60-90,i}$)	$\hat{\beta}_0$ [equations (7)–(9)]	$\hat{\sigma}^2$ [equations (10)–(12)]
0–30	137	0.91	24.38	18.13	−2.189	−1.659	0.1201
	581	2.99	40.00	30.13	−1.393		
	1178	2.25	29.00	25.00	−1.590		
	1451	2.72	30.88	26.38	−1.438		
	2100	1.42	20.63	21.00	−1.986		
	2379	4.16	38.75	38.38	−1.361		
30–60	137	0.91	24.38	18.13	−3.703	−3.383	0.0438
	581	3.00	40.00	30.13	−3.133		
	1178	1.65	29.00	25.00	−3.481		
	1451	2.26	30.88	26.38	−3.234		
	2100	1.30	20.63	21.00	−3.480		
	2379	3.38	38.75	38.38	−3.270		
60–90	137	1.68	24.38	18.13	−2.972	−2.993	0.2171
	581	1.70	40.00	30.13	−3.509		
	1178	1.48	29.00	25.00	−3.310		
	1451	3.89	30.88	26.38	−2.412		
	2100	1.05	20.63	21.00	−3.298		
	2379	4.87	38.75	38.38	−2.457		

Polled MSPE = 1/3(0.1201 + 0.0438 + 0.2171) = 0.127 = Grade A (excellent). EC_e, electrical conductivity of the saturation extract (dS m^{-1}); EM_h, apparent soil electrical conductivity measured with electromagnetic induction in the horizontal coil configuration (dS m); EM_v, apparent soil electrical conductivity measured with electromagnetic induction in the vertical coil configuration (dS/m).

will cause yield decrements of moderately salt-sensitive crops. To get good yields (i.e., relative crop yield >90%) of high valued salt sensitive crops (i.e., salinity threshold of <1.5 dS/m) leaching of the field is needed particularly the eastern half and northwest corner. After sufficient leaching is conducted to bring root zone EC_es below 2 dS/m, salt-sensitive crops such as carrots, beans (common and mung) and strawberries can be grown with good yields.

Conclusion

The compiled database consisting of data from 77 fields provided an excellent representation of EM38 survey conditions encountered in the Coachella Valley. The database contained fields across a wide area of the valley with considerable crop and irrigation management diversity and a range of lighter textured soils that typify the Coachella Valley. Not surprisingly, more than 50% of the soil samples exhibited EC_e less than 3 dS/m, but about 10% of the samples exceeded 10 dS/m. The correlation levels between the log transformed EC_e and log transformed EM38 signal data (i.e., EC_a) were moderate to high (r = 0.6 to 0.8) and the field specific DPPC correlation coefficients suggested that the majority of the survey data exhibited a high degree of internal consistency and reliability. However, there appeared to be a stronger than normal water content influence on the EM38 signal data in 10 of the 77 fields, which is consistent with typical surveying conditions encountered in the valley because of the prevalence of lighter textured soils. Nevertheless, the compiled database provided a robust and realistic dataset to validate the ANOCOVA modelling approach.

Based on accuracy of salinity prediction, the ANOCOVA approach outperformed FSR and CCR. The results show that the ANOCOVA modelling approach improves the accuracy of soil salinity predictions from EM38 signal data, particularly in fields where a limited number of calibration sampling locations are available.

Only one parameter estimate for each field is needed for ANOCOVA, rather than three for FSR, resulting in greater estimation precision and increased model stability. In addition, the ANOCOVA approach requires less sample data per field once the basic ANOCOVA models have been developed. The field-specific intercept estimates in the ANOCOVA modelling approach successfully adjust for the majority of field specific effects that tend to shift EC_a data patterns multiplicatively from one field to the next under a log transformation.

The extensive Coachella Valley dataset validated the ANOCOVA modelling approach as a viable regional-scale

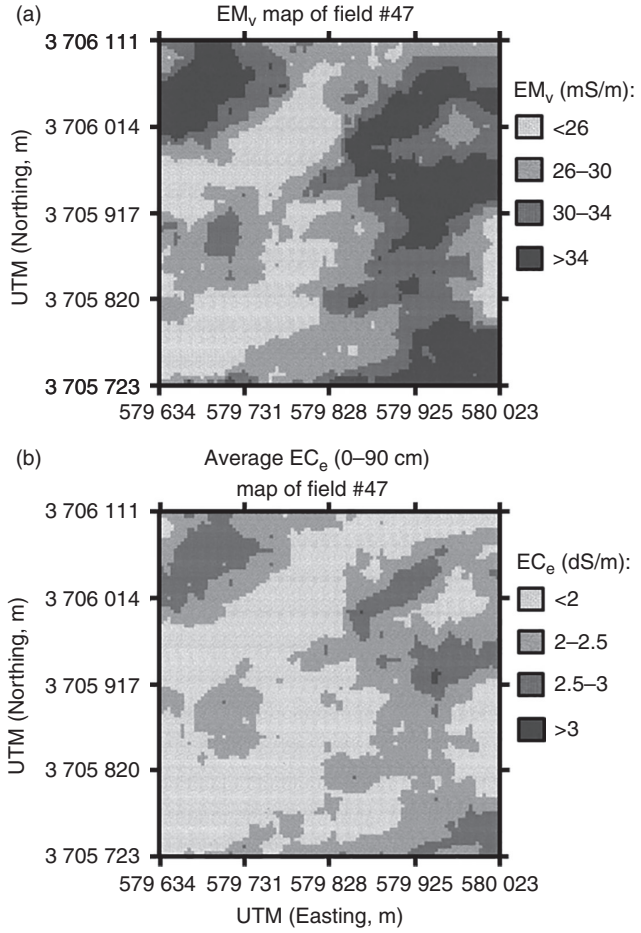

Figure 6 Maps of Field #47 for (a) electromagnetic induction apparent soil electrical conductivity taken in the vertical configuration (EM_v) and (b) average soil salinity (electrical conductivity of the saturation extract, EC_e, dS/m) for the 0–90 cm depth increment.

calibration technique. The ANOCOVA approach is a compromise between calibrating a regression model for each field and calibrating a model across all fields in the survey area (Corwin & Lesch, 2014).

A comparison of the ANOCOVA approach to another recent approach for mapping salinity at regional scale provides insight into the strengths, limitations, and appropriate scale of application of the ANOCOVA approach. The most recent and robust approach for regional-scale mapping of soil salinity is by Scudiero *et al.* (2015), which builds on the work of Lobell *et al.* (2010). Scudiero *et al.* (2015) use Landsat 7 ETM+ canopy reflectance and the Canopy Response Salinity Index in combination with EC_a-directed soil sampling (Corwin & Lesch, 2005b, 2013) to map the entire west side of California's San Joaquin Valley. A comparison of the ANOCOVA approach to the remote imagery approach of Scudiero *et al.* (2015) shows that the ANOCOVA approach provides greater accuracy and higher resolution, but at the expense of higher cost and greater labour requirements. Even though the ANOCOVA approach could be used at regional scale (10–10^5 km^2), its greater demand on resources and greater accuracy and resolution make it more appropriate for landscape scale (1–10 km^2) application, whereas the remote imagery approach of Lobell *et al.* (2010) and Scudiero *et al.* (2015) is clearly best for regional-scale application.

Acknowledgements

Funding of work was in part by a grant with Coachella Valley Resource Conservation District (agreement #09FG340003) and by a grant with the Office of Naval Research (agreement #60-0202-3-001). The authors wish to acknowledge Silvia Aslan and Susano Duarte from the Coachella Valley Resource Conservation District for their involvement and effort related to the soil salinity surveys within the Lower Colorado Region.

References

Bouaziz, M., Matschullat, J. & Gloaguen, R. 2011. Improved remote sensing detection of soil salinity from a semi-arid climate in Northeast Brazil. *Comptes Rendus Geoscience*, **343**, 795–803.

Caccetta, P., Dunne, R., George, R. & McFarlane, D. 2010. An estimate of the future extent of dryland salinity in the Southwest of Western Australia. *Journal of Environmental Quality*, **39**, 26–34.

Corwin, D.L. & Lesch, S.M. 2003. Application of soil electrical conductivity to precision agriculture: theory, principles, and guidelines. *Agronomy Journal*, **95**, 455–471.

Corwin, D.L. & Lesch, S.M. 2005a. Apparent soil electrical conductivity measurements in agriculture. *Computers & Electronics in Agriculture*, **46**, 11–43.

Corwin, D.L. & Lesch, S.M. 2005b. Characterizing soil spatial variability with apparent soil electrical conductivity: I. Survey protocols. *Computers & Electronics in Agriculture*, **46**, 103–133.

Corwin, D.L. & Lesch, S.M. 2013. Protocols and guidelines for field-scale measurement of soil salinity distribution with EC_a-directed soil sampling. *Journal of Environmental and Engineering Geophysics*, **18**, 1–25.

Corwin, D.L. & Lesch, S.M. 2014. A simplified regional-scale electromagnetic induction – salinity calibration model using ANOCOVA modeling techniques. *Geoderma*, **230–231**, 288–295.

Dang, Y.P., Pringle, M.J., Schmidt, M., Dalal, R.C. & Apan, A. 2011. Identifying the spatial variability of soil constraints using multi-year remote sensing. *Field Crops Research*, **123**, 248–258.

Furby, S.L., Caccetta, P. & Wallace, J.F. 2010. Salinity monitoring in Western Australia using remotely sensed and other spatial data. *Journal of Environmental Quality*, **39**, 16–25.

Harvey, O.R. & Morgan, C.L.S. 2009. Predicting regional-scale soil variability using a single calibrated apparent soil electrical conductivity model. *Soil Science Society of America Journal*, **73**, 164–169.

Ivits, E., Cherlet, M., Tóth, T., Lewińska, K.E. & Tóth, G. 2013. Characterization of productivity limitation on salt-affected lands indifferent climatic regions of Europe using remote sensing derived productivity indicators. *Land Degradation & Development*, **24**, 438–452.

Lesch, S.M. & Corwin, D.L. 2003. Using the dual-pathway parallel conductance model to determine how different soil properties influence conductivity survey data. *Agronomy Journal*, **95**, 365–379.

Lesch, S.M., Rhoades, J.D. & Corwin, D.L. 2000. *ESAP-95 Version 2.10R: User Manual and Tutorial Guide*, Research Rpt. 146. USDA-ARS, U.S. Salinity Laboratory, Riverside, CA, USA.

Lobell, D.B., Lesch, S.M., Corwin, D.L., Ulmer, M.G., Anderson, K.A., Potts, D.J., Doolittle, J.A., Matos, M.R. & Baltes, M.J. 2010. Regional-scale assessment of soil salinity in the Red River Valley using multi-year MODIS EVI and NDVI. *Journal of Environmental Quality*, **39**, 35–41.

Massoud, F.I. 1981. Salt affected soils at a global scale and concepts for control. FAO Land and Water Development Div., Technical Paper: Food and Agriculture Organization of the United Nations, Rome, Italy, 21 pp.

Rhoades, J.D. 1996. Salinity: Electrical conductivity and total dissolved solids. In: *Methods of Soil Analysis: Part 3 – Chemical Methods* (ed. D.L. Sparks), pp. 417–435. SSSA Book Series No. 5. Soil Sci. Soc. Am., Madison, WI.

Scudiero, E., Skaggs, T.H. & Corwin, D.L. 2015. Regional-scale soil salinity assessment using Landsat ETM+ canopy reflectance. *Remote Sensing of Environment*, **169**, 335–343.